Compound Gauss Markov Random Fields for Astronomical Image Restoration

Molina, R.,[a] Katsaggelos, A. K.,[b] Mateos, J.[a] and Abad, J.[a]

[a] *Departamento de Ciencias de la Computación e Inteligencia Artificial*
Universidad de Granada.
18071 Granada. España.

[b] *Department of Electrical Engineering and Computer Science*
Northwestern University.
Evanston, IL 60208.

Abstract

Over the last few years, a growing number of researchers from varied disciplines have been utilizing Markov random fields (MRF) models for developing optimal, robust algorithms for various problems, such as texture analysis, image synthesis, image restoration, classification and segmentation, surface reconstruction, integration of several low level vision modules and sensor fusion. While linear-shift invariant (LSI) models have been generally used for image restoration in astronomy, no much work has been reported on the use of more complex models in this area.

In this paper we examine the use of Compound Gaussian Markov Random Fields, (CGMRF), a non LSI model that preserves image discontinuities, to restore astronomical images. Problems on the application of the model arising from the high dynamic range and severe blurring of astronomical images are addressed and two new methods to estimate the real underlying image are proposed. The methods are tested on real astronomical images.

1 Introduction

Image restoration refers to the problem of recovering an image, $\mathbf{f}$, from its blurred and noisy observation, $\mathbf{g}$, for the purpose of improving its quality or obtaining some type of information that is not readily available from the degraded image.

It is well known that translation invariant linear image models are not, in many circumstances, the more appropriate restoration methods. Their main problem is their lack to preserve the discontinuities. To move from simple LSI

models several methods have been applied in astronomy. Among them, Starck and colleagues [4,4] use multiresolution techniques based on wavelet decomposition, Geman and Yang [4] use the minimization on an auxiliary array and an extended objective function in which the original variables appear quadratically and the auxiliary variables are decoupled, Núñez and Llacer [4] segment the images on regions with similar statistical properties and assign a different variance to each region, Kang and Katsaggelos [4,4] adapt the parameters in the model locally, Lucy [4] uses the observer-supplied information about sources that are naturally taken to be point sources and treats them consequentially and Molina et al. [4] introduce a region process supposing that the location of the objects in the image is known in advance and assign different properties to the different regions.

The CGMRF theory provides us a way to control the change on the image model using a hidden random field. So, a compound random field has two levels, an upper level that is the real image that has some translation invariant lineal sub-models to represent some image characteristics like border region, smoothness, texture, etc. The lower or hidden level is a finite range random field to govern the transitions between the sub-models. The use of the underlying random field, called line process, was introduced by Geman and Geman in [4].

Given the image and the noise models, the process of finding the maximum a posteriori (MAP) for the CGMRF is much more complex since we no longer have a convex function to be minimized and methods like simulated annealing (see Geman and Geman in [4]) have to be used. Although this method leads to the MAP, it is a high computational demanding method. A faster alternative is the converging algorithm called deterministic relaxation used to obtain a local MAP estimation. This method is also called *iterative conditional mode* (ICM) [4].

In this paper we present the application of CGMRF to image restoration in astronomy. In section 2 we introduce the used notation and the proposed model for the image and line processes as well as the noise models. Both, stochastic and deterministic relaxation approach to estimate the MAP are presented in section 3. In section 4 we work on the problems on the application of the model on astronomical images due to the high dynamic range and severe blurring present and two new methods to estimate the real underlying image are proposed. Finally, in section 5 we test both algorithms on real astronomical images.

2 Notation and Model

2.1 Bayesian model

We will distinguish between $\mathbf{f}$, the 'true' image which would be observed under ideal conditions and $\mathbf{g}$, the observed image. The aim is to reconstruct $\mathbf{f}$ from $\mathbf{g}$. Bayesian methods start with a prior distribution, a probability distribution over images $\mathbf{f}$ by which they incorporate information on the expected structure within an image. It is also necessary to specify $\mathrm{p}(\mathbf{g} \mid \mathbf{f})$, the probability distribution of observed images $\mathbf{g}$ if $\mathbf{f}$ were the 'true' image. The Bayesian paradigm dictates that the inference about the true $\mathbf{f}$ should be based on $\mathrm{p}(\mathbf{f} \mid \mathbf{g})$ given by

$$\mathrm{p}(\mathbf{f} \mid \mathbf{g}) = \mathrm{p}(\mathbf{g} \mid \mathbf{f})\mathrm{p}(\mathbf{f})/\mathrm{p}(\mathbf{g}) \propto \mathrm{p}(\mathbf{g} \mid \mathbf{f})\mathrm{p}(\mathbf{f}). \tag{1}$$

Maximization of (1) with respect to $\mathbf{f}$ yields

$$\hat{\mathbf{f}} = \arg\max_{\mathbf{f}} \mathrm{p}(\mathbf{f} \mid \mathbf{g}), \tag{2}$$

the maximum-a-posteriori (MAP) estimator. For the sake of simplicity, we will denote by $\mathbf{f}_i$ the intensity of the true image at the location of the pixel i on the lattice. We regard $\mathbf{f}$ as a $p \times 1$ column vector of values $\mathbf{f}_i$. The convention applies equally to the observed image $\mathbf{g}$.

2.2 Incorporation of the edges location in the prior model

The use of CGMRF was first presented in [4] using an Ising model to represent the upper level and a line process to model the abrupt transitions. Extensions to continuous range models using GMRF were presented in [4]. The CGMRF model used in this paper was proposed by Chellapa, Simchony and Lichtenstein in [4] and it is an extension of the Blake and Zisserman's weak membrane model [4] used for surface interpolation and edge detection.

Let us now introduce the CGMRF model from the simpler model, the Conditional Autoregression (CAR). The idea is to build a prior model consisting of two processes, one accounting for the intensity values and the other for the location of edges in the image.

Let us first describe the prior model without any edges. Our prior knowledge about of the smoothness of the object luminosity distribution makes it possible

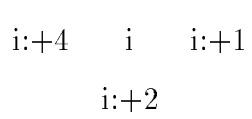

Fig. 1. The neighborhood system

to model the distribution of $\mathbf{f}$ by a conditional autoregression (CAR) (see Ripley [4]). Thus,

$$\mathrm{p}(\mathbf{f}) \propto \exp\left\{-\frac{1}{2\sigma_{\mathrm{w}}^2}\mathbf{f}^{\mathrm{T}}(\mathbf{I}-\phi\mathbf{N})\mathbf{f}\right\} \tag{3}$$

where $\mathbf{N}_{ij} = 1$ if cells i and j are spatial neighbors (pixels at distance one), zero otherwise and $\phi = 0.25$. The term $\mathbf{f}^{\mathrm{T}}(\mathbf{I}-\phi\mathbf{N})\mathbf{f}$ represents in matrix notation the sum of squares of the values $\mathbf{f}_i$ minus ϕ times the sum of $\mathbf{f}_i\mathbf{f}_j$ for neighboring pixels i and j. The parameters can be interpreted by the following expressions describing the conditional distribution

$$\mathrm{E}(\mathbf{f}_i \mid \mathbf{f}_j,\ j \neq i) = \phi \sum_{j\ \mathrm{nhbr}\ i} \mathbf{f}_j \qquad \mathrm{var}(\mathbf{f}_i \mid \mathbf{f}_j,\ j \neq i) = \sigma_{\mathrm{w}}^2 \tag{4}$$

where the suffix 'j nhbr i' denotes the four neighbor pixels at distance one from pixel i. The parameter σ_{w}^2 measures the smoothness of the 'true' image.

From (3) we have

$$-\log \mathrm{p}(\mathbf{f}) = \mathrm{const} + \sum_i \mathbf{f}_i(\mathbf{f}_i - \phi(\mathbf{N}\mathbf{f})_i)/2\sigma_{\mathrm{w}}^2 \tag{5}$$

Then, if i:+1, i:+2, i:+3, i:+4 denote the four pixels around pixel i as described in the figure 1 and we assume a 'toroidal edge correction', we have

$$-\log \mathrm{p}(\mathbf{f}) = \mathrm{const} + \left[\sum_i \phi(\mathbf{f}_i - \mathbf{f}_{i:+1})^2 + \sum_i \phi(\mathbf{f}_i - \mathbf{f}_{i:+2})^2\right]/2\sigma_{\mathrm{w}}^2. \tag{6}$$

This expression can be rewritten as

$$\begin{aligned} -\log \mathrm{p}(\mathbf{f},\mathbf{l}) = \mathrm{const} + \sum_i \Big[&\phi(\mathbf{f}_i - \mathbf{f}_{i:+1})^2(1-\mathbf{l}_{<i,i:+1>}) + \beta\mathbf{l}_{<i,i:+1>} \\ &+ \phi(\mathbf{f}_i - \mathbf{f}_{i:+2})^2(1-\mathbf{l}_{<i,i:+2>}) + \beta\mathbf{l}_{<i,i:+2>}\Big]/2\sigma_{\mathrm{w}}^2 \end{aligned} \tag{7}$$

where $\mathbf{l}_{<i,j>} \equiv 0$ for all i and j.

We then introduce a line process by simply redefining the function $\mathbf{l}_{<i,j>}$ as taking the value zero if pixels i and j are not separated by an active line and one otherwise and then, penalizing the introduction of the line element by the term $\beta \mathbf{l}_{<i,j>}$. The intuitive interpretation of this line process is simple; it acts as an activator or inhibitor of the relation between two neighbor pixels depending on whether both pixels are separated or not by an edge.

2.3 Noise models

The main sources of noise are the discrete nature of photons and electronic noise in the CCD detector. Physical considerations suggest that this noise is independent from pixel to pixel and depending on the average number of photons arriving at the CCD cell. A simplified noise model is to assume that it is Gaussian with mean zero and variance σ_{n}^2. That means that the observed image corresponds to the model $\mathbf{g}_i = (\mathbf{Df})_i + \mathbf{n}_i = \sum_j d_{i-j}\mathbf{f}_j$ where $\mathbf{D}$ is the $p \times p$ matrix defining the systematic blur, assumed to be known and approximated by a block circulant matrix, $\mathbf{n}_i$ is additive Gaussian noise with zero mean and variance σ_{n}^2 and d_j are the coefficients defining the blurring function.

Then, the probability of the observed image $\mathbf{g}$ if $\mathbf{f}$ were the 'true' image is

$$\mathrm{p}(\mathbf{g} \mid \mathbf{f}) \propto \exp\left[-\frac{1}{2\sigma_{\mathrm{n}}^2}\left\|\mathbf{g} - \mathbf{Df}\right\|^2\right]. \tag{8}$$

A more realistic model for the noise is $\mathbf{g}_i \sim \mathcal{P}((\mathbf{Df})_i)$. This model can be approximated, at least for high brightness values, by the Gaussian distribution $\mathcal{N}((\mathbf{Df})_i, (\mathbf{Df})_i)$ and, then, the probability of the observed image $\mathbf{g}$ if $\mathbf{f}$ were the 'true' image is

$$\mathrm{p}(\mathbf{g} \mid \mathbf{f}) \propto \exp\left[-\sum_i \frac{(\mathbf{g}_i - (\mathbf{Df})_i)^2}{(\mathbf{Df})_i}\right]. \tag{9}$$

3 Stochastic and Deterministic Relaxation for Estimating the MAP

Let us now proceed to find $\hat{\mathbf{f}}$, $\hat{\mathbf{l}}$, the MAP estimate of $\mathbf{f}$ and $\mathbf{l}$, that is

$$\hat{\mathbf{f}}, \hat{\mathbf{l}} = \arg\max_{\mathbf{f},\mathbf{l}} \mathrm{p}(\mathbf{f}, \mathbf{l} \mid \mathbf{g}). \tag{10}$$

This is an obvious extension of the equation (2) where we now have the image and the line process. The simulated annealing algorithm ensures us conver-

gence to the global MAP estimate regardless of the initial solution. It is based on the way in which some chemical systems reach the lowest energy – maximum stability states by a gradual lowering of the temperature. Deterministic relaxation is a faster alternative to the SA algorithm to obtain a local MAP estimation.

3.1 Finding the MAP using Simulated Annealing

Since $p(\mathbf{f},\mathbf{l} \mid \mathbf{g})$ is nonlinear it is extremely difficult to find $\hat{\mathbf{f}}$ and $\hat{\mathbf{l}}$ by any conventional method. Simulated Annealing is a relaxation technique to search for MAP estimates from degraded observations.

It uses the distribution

$$\begin{aligned} p_T(\mathbf{f},\mathbf{l} \mid \mathbf{g}) = \frac{1}{Z_T} \exp\Big\{ & -\frac{1}{T} U(\mathbf{g} \mid \mathbf{f}) \\ & - \frac{1}{T} \sum_i \Big[\phi(\mathbf{f}_i - \mathbf{f}_{i:+1})^2 (1 - \mathbf{l}_{<i,i:+1>}) + \beta \mathbf{l}_{<i,i:+1>} \\ & + \phi(\mathbf{f}_i - \mathbf{f}_{i:+2})^2 (1 - \mathbf{l}_{<i,i:+2>}) + \beta \mathbf{l}_{<i,i:+2>} \Big] / 2\sigma_w^2 \Big\} \end{aligned} \tag{11}$$

where T is the temperature Z_T is a normalization constant and

$$U(\mathbf{g} \mid \mathbf{f}) = \frac{1}{2\sigma_n^2} \|\mathbf{g} - \mathbf{D}\mathbf{f}\|^2 \quad \text{or} \quad U(\mathbf{g} \mid \mathbf{f}) = \sum_i \frac{(\mathbf{g}_i - (\mathbf{D}\mathbf{f})_i)^2}{(\mathbf{D}\mathbf{f})_i} \tag{12}$$

depending on whether we use a Gaussian or the normal approximation to Poisson noise model, respectively and proceeds as follows.

Sequential simulated annealing procedure.

(i) Set $T = 1$. Set $k = 0$.
(ii) Let u denote sites in the line process. For each site, u, simulate its posterior probability distribution, $p_T(\mathbf{l}_u \mid \text{rest of } \mathbf{l}, \mathbf{f}, \mathbf{g})$.
(iii) For each pixel i update $\mathbf{f}_i$ by simulating $p_T(\mathbf{f}_i \mid \text{rest of } \mathbf{f}, \mathbf{l}, \mathbf{g})$.
(iv) Set $k = k + 1$. Decrease the temperature T and go back to the step (ii) until k is greater than a specified number.

Note that the temperature only is decreased after a full sweep of the line process and the picture (after going through all lines and pixels and update them according to the algorithm). Conditions for the algorithm to converge to the MAP are established in [4,4].

Hence we have to simulate the conditional a posteriori density function for

$\mathbf{l}_{<i,j>}$, given the rest of $\mathbf{l}$, $\mathbf{f}$ and $\mathbf{g}$ and the conditional a posteriori density function for $\mathbf{f}_i$ given the rest of $\mathbf{f}$, $\mathbf{l}$ and $\mathbf{g}$. Lets us now examine these distributions.

In order to simulate the line process conditional a posteriori density function, $\mathrm{p_T}(\mathbf{l}_{<i,j>} \mid \text{rest of } \mathbf{l},\mathbf{f},\mathbf{g})$, we have

$$\mathrm{p_T}(\mathbf{l}_{<i,j>} = 0 \mid \text{rest of } \mathbf{l},\mathbf{f},\mathbf{g}) \propto \exp\left[-\frac{1}{T}\frac{\phi}{2\sigma_{\mathrm{w}}^2}(\mathbf{f}_i - \mathbf{f}_j)^2\right] \tag{13}$$

$$\mathrm{p_T}(\mathbf{l}_{<i,j>} = 1 \mid \text{rest of } \mathbf{l},\mathbf{f},\mathbf{g}) \propto \exp\left[-\frac{1}{T}\beta\right] \tag{14}$$

Furthermore, for Gaussian noise, $\mathrm{p_T}(\mathbf{f}_i \mid \text{rest of } \mathbf{f},\mathbf{l},\mathbf{g}) \sim \mathcal{N}(\mu_i, \sigma_i^2)$, where μ_i and σ_i are given by

$$\mu_i = \lambda_i \sum_{j\,\mathrm{nhbr}\,i} \frac{\mathbf{f}_j(1-\mathbf{l}_{<i,j>})}{nn_i} + (1-\lambda_i)\left(\frac{(\mathbf{D}^{\mathrm{T}}\mathbf{g})_i - (\mathbf{D}^{\mathrm{T}}\mathbf{D}\mathbf{f})_i}{c} + \mathbf{f}_i\right) \tag{15}$$

$$\frac{1}{\sigma_i^2} = \frac{1}{T}\left[\frac{nn_i\,\phi}{\sigma_{\mathrm{w}}^2} + \frac{c}{\sigma_{\mathrm{n}}^2}\right] \text{ and } \sigma_i^2 = \frac{T\sigma_{\mathrm{w}}^2\sigma_{\mathrm{n}}^2}{nn_i\,\phi\sigma_{\mathrm{n}}^2 + c\,\sigma_{\mathrm{w}}^2}. \tag{16}$$

where c is the sum of the square of the coefficients defining the blur function, that is, $c = \sum_j d_j^2$, $nn_i = \sum_{j\,\mathrm{nhbr}\,i}(1-\mathbf{l}_{<i,j>})$ and

$$\lambda_i = \frac{\frac{nn_i\,\phi}{\sigma_{\mathrm{w}}^2}}{\frac{nn_i\,\phi}{\sigma_{\mathrm{w}}^2} + \frac{c}{\sigma_{\mathrm{n}}^2}} = \frac{nn_i\,\phi\sigma_{\mathrm{n}}^2}{nn_i\,\phi\sigma_{\mathrm{n}}^2 + c\,\sigma_{\mathrm{w}}^2}. \tag{17}$$

If we use the normal approximation to Poisson noise model, the conditional distribution, $\mathrm{p_T}(\mathbf{l}_{<i,j>} \mid \text{rest of } \mathbf{l},\mathbf{f},\mathbf{g})$ is the same as in (13) and (14) and, if we approach the noise model by the Gaussian, then

$$\mathrm{p}(\mathbf{f}_i \mid \text{rest of } \mathbf{f},\mathbf{l},\mathbf{g}) = \frac{1}{\sqrt{2\pi}\sigma_i}\exp\left[-\frac{1}{2\sigma_i^2}(\mathbf{f}_i - \mu_i)^2\right], \tag{18}$$

where

$$\mu_i = \lambda_i \sum_{j\,\mathrm{nhbr}\,i} \frac{\mathbf{f}_j(1-\mathbf{l}_{<i,j>})}{nn_i} + \sum_j \gamma_{i,j}\left(\frac{\mathbf{g}_{i+j} - (\mathbf{D}\mathbf{f})_{i+j}}{d_j} + \mathbf{f}_i\right) \tag{19}$$

$$\frac{1}{\sigma_i^2} = \frac{1}{T}\left[\frac{nn_i\,\phi}{\sigma_{\mathrm{w}}^2} + \sum_j \frac{d_j^2}{(\mathbf{D}\mathbf{f})_{i+j}}\right] \text{ and } \sigma_i^2 = \frac{T}{\frac{nn_i\,\phi}{\sigma_{\mathrm{w}}^2} + \sum_j \frac{d_j^2}{(\mathbf{D}\mathbf{f})_{i+j}}} \tag{20}$$

where

$$\lambda_i = \frac{\frac{nn_i\,\phi}{\sigma_{\mathrm{w}}^2}}{\frac{nn_i\,\phi}{\sigma_{\mathrm{w}}^2} + \sum_j \frac{d_j^2}{(\mathbf{Df})_{i+j}}} \quad \text{and} \quad \gamma_{i,j} = \frac{\frac{d_j^2}{(\mathbf{Df})_{i+j}}}{\frac{nn_i\,\phi}{\sigma_{\mathrm{w}}^2} + \sum_k \frac{d_k^2}{(\mathbf{Df})_{i+k}}} \tag{21}$$

Here we neglect the contribution from $\sum_j [d_j(\mathbf{g}_{i+j} - (\mathbf{Df})_{i+j})^2]/2(\mathbf{Df})_{i+j}^2$ to the mean and variance.

3.2 Deterministic Relaxation Approach

Instead of using a stochastic approach, we can use a deterministic method to search for a local maximum. An advantage of the deterministic method is that its convergence is much faster than the stochastic approach since instead of simulating the distributions always takes the mode from the corresponding conditional distribution The disadvantage is the local nature of the solution obtained. This method can be seen as a particular case of simulated annealing where the temperature is always set to zero.

4 Unstability of the SA and ICM Solutions

The iterative methods previously described may not converge, as described in [4], since, if we suppose for simplicity no line process and we update the whole image an the same time we have, assuming Gaussian noise

$$\begin{aligned}
\mathbf{f}^k &= \lambda\phi\mathbf{N}\mathbf{f}^{k-1} - (1-\lambda)\left[\frac{\mathbf{D}^{\mathrm{T}}\mathbf{D}}{c}\mathbf{f}^{k-1} - \mathbf{f}^{k-1}\right] + (1-\lambda)\frac{\mathbf{D}^{\mathrm{T}}\mathbf{g}}{c} \\
&= \mathbf{f}^{k-1} - \lambda(\mathbf{I} - \phi\mathbf{N})\mathbf{f}^{k-1} - (1-\lambda)\frac{\mathbf{D}^{\mathrm{T}}\mathbf{D}}{c}\mathbf{f}^{k-1} + \text{const} \\
&= \mathbf{A}\mathbf{f}^{k-1} + \text{const}
\end{aligned} \tag{22}$$

where the superscript k is the iteration number and

$$\mathbf{A} = \left[\mathbf{I} - \lambda(\mathbf{I} - \phi\mathbf{N}) - (1-\lambda)\frac{\mathbf{D}^{\mathrm{T}}\mathbf{D}}{c}\right]. \tag{23}$$

In order for the method to converge $\mathbf{A}$ must be a contraction. However this may not be the case for severe blurring and high dynamic range images.

To solve this problem, when dealing with Gaussian noise, we use the value of $\mathbf{f}_i$ obtained in the previous iteration, $\mathbf{f}_i^{\text{old}}$, and, instead of simulating from the normal distribution defined in (15), (16) to obtain the new value of $\mathbf{f}_i$, we simulate from the normal distribution with mean

$$\mu_i' = \omega_i \mathbf{f}_i^{\text{old}} + (1 - \omega_i)\mu_i \tag{24}$$

with $\omega_i = (1-c)\sigma_{\mathbf{w}}^2/(nn_i\,\phi\,\sigma_{\mathbf{n}}^2 + \sigma_{\mathbf{w}}^2)$.

In this case, it can be observed that the corresponding $\mathbf{A}$ matrix is given by

$$\mathbf{A} = \left[\mathbf{I} - \lambda(\mathbf{I} - \phi\mathbf{N}) - (1-\lambda)\mathbf{D}^{\mathrm{T}}\mathbf{D}\right] \tag{25}$$

which is a contraction.

Having the same convergence problem for the Poisson noise model, it is solved analogously to the Gaussian noise case and, instead of simulating from the normal distribution defined in (19), (20) to obtain the new value of $\mathbf{f}_i$, we simulate from the normal distribution with mean

$$\mu_i' = \omega_i \mathbf{f}_i^{\text{old}} + (1 - \omega_i)\mu_i \tag{26}$$

with

$$\omega_i = \frac{\sum_j \frac{d_j - d_j^2}{(\mathbf{Df})_{i+j}}}{\frac{nn_i\,\phi}{\sigma_{\mathbf{w}}^2} + \sum_j \frac{d_j}{(\mathbf{Df})_{i+j}}}. \tag{27}$$

5 Results

The methods were tested on images of Saturn which were obtained at the Cassegrain f/8 focus of the 1.52-m telescope at Calar Alto Observatory (Spain) on July, 1991. Results are presented on a image, figure 2a, taken through a narrow-band interference filter centered at the wavelength 9500 Åwith a range of $[100, 6100]$ photons.

The blurring function, $\mathbf{D}$ can be approximated by

$$d_i \propto \left(1 + \frac{i^2}{R^2}\right)^{-\delta}. \tag{28}$$

The parameters δ and R were estimated from the intensity profiles of satellites of Saturn that were recorded simultaneously with the planet and of stars that

figure2a.ps figure2b.ps figure2c.ps

Fig. 2. From left to right: Observed image. Restorations with original ICM and SA method, Gaussian noise model.

were recorded very close in time and airmass to the planetary images. We found $\delta \sim 3$ and $R \sim 3.4$ pixels. The PSF used on the tests is a 23×23 approximation due to the high time demanded by the methods.

The noise variance for the Gaussian noise model were estimated from the data using MLE, finding $\sigma_{\mathrm{n}}^2 = 125$. The parameter β and the prior variance were estimated experimentally and $\beta = 50$ and $\sigma_{\mathrm{w}}^2 = 2000$ were used. Results for the original ICM and SA methods with Gaussian noise model after 100 and 2000 iterations respectively are depicted on the figure 2b and c. The range of these images are [0, 11550] and [0, 15886] for the ICM and SA method respectively presenting some spikes due to the methods unstability. Figure 3 depicts the resulting image and line process after running our proposed ICM and SA methods for Gaussian noise with the previous parameters, for 100 and 2000 iterations respectively. The range of these images are [0, 7405] for the ICM method and [0, 7416] for SA. Figure 4 depicts the resulting image and line process after running our proposed ICM and SA methods for the normal approximation to Poisson noise model with $\sigma_{\mathrm{w}}^2 = 12500$ and $\beta = 7$ for 100 and 2000 iterations respectively. In all the images the improvement in spatial resolution is evident.

To examine the quality of the MAP estimate of the line process we compared it with the position of the ring and disk of Saturn, obtained from the Astronomical Almanac, corresponding to out observed image. Although all the methods detect a great part of the ring and the disk, the ICM method, both with Gaussian and normal approximation to Poisson noise, figure 5 (a) and (b) respectively, shows thick lines. The SA method, on the other hand, give us thinner lines and the details are more resolved both with Gaussian and normal approximation to Poisson noise, figure 5 (c) and (d) respectively. Obviously there are some gaps in the line process but continuity of this process could be imposed if we added more terms.

figure3a.ps figure3b.ps figure3c.ps figure3d.ps

Fig. 3. From left to right: Restoration with the proposed ICM method, its line process, restoration with the proposed SA method and its line process, Gaussian noise model

figure4a.ps figure4b.ps figure4c.ps figure4d.ps

Fig. 4. From left to right: Restoration with proposed ICM method, its line process, restoration with proposed SA method and its line process, normal approximation to Poisson noise model

figure5a.ps figure5b.ps figure5c.ps figure5d.ps

Fig. 5. Comparation between the real edges (dark) and the obtained line process (light).

References

[1] Besag, J. (1986), "On the Statistical Analysis of Dirty Pictures", *J. Royal Statistics Soc.* B **48**, 259–302.

[2] Blake, A. and Zisserman, A. (1987), "Visual Reconstruction", Cambridge, MIT Press.

[3] Chellapa, R., Simchony, T. and Lichtenstein, Z. (1991), "Image Estimation Using 2D Noncausal Gauss-Markov Random Field Models", in *Digital Image Restoration*, Katsaggelos, A.K. (ed.), Springer Series in Information Science, vol. 23, Springer–Verlag.

[4] Geman, S., Geman D. (1984), "Stochastic Relaxation, Gibbs Distributions, and the Bayesian Restoration of Images", *IEEE Trans. on PAMI*, vol. PAMI-9, (**6**), 721–742.

[5] Geman D. and Yang, C. (1995), "Nonlinear Image Recovery with Half-Quadratic Regularization", *IEEE Trans. on IP*, **4**, 7, 932–946.

[6] Jeng, F.C., and Woods, J.W. (1988), "Simulated Annealing in Compound Gaussian Random Fields", *IEEE Trans. Inform. Theory*, **36**, 94–107.

[7] Jeng, F.C. and Woods, J.W. (1988), "Image estimation by stochastic relaxation in the compound Gaussian case", in *Proc. IEEE Inter. Conf. ASSP.*

[8] Kang, M.G., Katsaggelos, A.K., (1994), "Frequency Domain Iterative Image Restoration and Evaluation of the Regularization Parameter", *Optical Engineering*, **33**, 10, 3222–3233.

[9] Katsaggelos, A.K., Kang, M.G. and Banham, M.R., (1994), "Adaptive Regularized Restoration Applied to HST Images", in *The Restoration of HST Images and Spectra II*, Hanisch, R.J., White, R.L. eds. STScI.

[10] Lucy L.B., (1994), "Image Restorations of High Photometric Quality", (1995) in *The Restoration of HST Images and Spectra II*, Hanisch, R.J., White, R.L. eds. STScI.

[11] Molina, R., Katsaggelos, A.K., Mateos, J. "CGMRF for High Dynamic Range Images" in preparation.

[12] Molina, R., Ripley, B.D., Molina, A., Moreno, F. and Ortiz, J.L. (1992), "Bayesian Deconvolution with Prior Knowledge of Object Location: Applications to Ground-Based Planetary Images", *AJ*, **104**, 1662–1668.

[13] Núñez, J and Llacer, J. (1995), "Variable Resolution Bayesian Image Reconstruction", in *Proc. IEEE Inter. Workshop on Nonlinear Signal and Image Processing*, 106–110.

[14] Ripley, B.D. (1981) "Spatial Statistics", Wiley, New York.

[15] Starck, J.-L. and Bijaoui, A., (1994), "Filtering and Deconvolution by the Wavelet Transform", *Signal Processing* **35** 195–211.

[16] Starck, J.-L. and Murtagh, F., (1994), "Image Restoration With Noise Suppression Using the Wavelet Transform" *A&A*, **288**, 343–348.